Multi-body dynamics modeling and test of an articulated steering half-track tractor

Baocheng Zhou[1], Shiyu Chen[1], Jianing Hu[2], Yong You[1], Decheng Wang[1], Qing Zhang[1*]

(1. *College of Engineering, China Agricultural University, Beijing 100083, China*;
2. *Shijiazhuang Xinnong Machinery Co., Ltd., Shijiazhuang 050000, China*)

Abstract: With the benefits of small turning radius and high trafficability, the articulated steering half-track tractor had been widely utilized in orchard and small spaced farmland. To study the dynamic performance of the articulated steering half-track tractor and provide a model basis for studying the path tracking control, an accurate multi-body dynamic model of the tractor was required. In this study, the crucial parameters in the dynamic model construction of the tractor were investigated. Firstly, the topology model of the components of the half-track tractor was built by RecurDyn, in which the movement subs and driver functions were given. Secondly, considering the difference of dynamic characteristic of the articulated steering tractor with respect to different pavement hardnesses, the soft and hard pavement models were constructed by employing the harmonic superposition method. Finally, the simulations of the half-track tractor under straight-line and swerve had been conducted on the two types of pavements, and the simulation results were compared with the experimental and theoretical results. The results indicated that the average speed error of the dynamic model on hard pavement and farmland soft pavement were 2.7% and 2.1% compared with the real tractor tests. At the same time, the straight-line driving offset errors of the dynamic model on the two pavements were 1.6% and 3.8% for the front wheels and the rear wheels offset errors were 3.9% and 2.4%, respectively. Furthermore, the turning radius error under front wheel steering was 8.2% and the error under articulated steering was 5.3%. It is proved that the established dynamic model had high accuracy, which provides an efficient approach to analyze the dynamic features of the half-track tractor.

Keywords: articulated steering, half-track tractor, multi-body dynamics, model verification, real tractor test
DOI: 10.25165/j.ijabe.20231606.8165

Citation: Zhou B C, Chen S Y, Hu J N, You Y, Wang D C, Zhang Q. Multi-body dynamics modeling and test of an articulated steering half-track tractor. Int J Agric & Biol Eng, 2023; 16(6): 124–133.

1 Introduction

The articulated steering tractor has the characteristics of small and compact structure, excellent trafficability and small turning radius, which has been widely utilized in orchards and small spacing farmland[1,2]. Meanwhile, with the rapid development of satellite navigation, wireless transmission of information, sensors and control technologies, the technical research and application of autonomous navigated agricultural equipment has also been rapidly promoted[3,4]. Unmanned driving technology for tractors has become an urgent research topic. Since the articulated steering tractor has special kinematics and dynamics characteristics, it is essential to establish an accurate simulation model for dynamic analysis[5-8].

Virtual prototype technology based on multi-body dynamics provides an excellent technical support for the kinematics and dynamics analysis of tracked vehicles[9,10]. Hu et al.[11] analyzed the movement process of the highland gap triangular crawler chassis during traveling and climbing by establishing the topological structure model of the crawler chassis. The results indicated that the constructed multi-body dynamics model of the highland gap triangular crawler chassis had high accuracy, which can provide support for dynamic analysis and optimization of crawler chassis. Similarly, Liu et al.[12,13] established the multi-body dynamics model of a small agricultural crawler chassis by using RecurDyn. By comparing the simulation and test data of the driving force torque, running speed, crawler tension and other parameters of the model, the effectiveness and accuracy of the simulation model were verified. Ma et al.[14] conducted research on high-speed tracked vehicles and developed a multi-body dynamics model of the entire vehicle using RecurDyn. The simulation was employed to obtain the track tension and normal force of the bearing wheel, and these results were agreement with the theoretical calculation results. As a result, this study provided a foundational model for controlling the tensioning force of the track driving system, highlighting its potential value in practical applications. Hao et al.[15,16] analyzed the topological structure of tanks and a multi-body dynamic model was established based on virtual prototype technology. Subsequently, a random pavement model was developed using harmonic superposition method. Finally, the reliability of the tank model was verified by comparing the results of simulation and test, which demonstrated that the multi-body dynamic model of the tank can accurately reflect the vibration characteristics of the actual tank. Wu et al.[17] developed a hydro-mechanical continuously variable transmission prototype. In order to evaluate its dynamic performance and speed ratio control, a dynamic model was

Received date: 2023-02-01 **Accepted date:** 2023-06-20
Biographies: Baocheng Zhou, PhD candidate, research interest: agricultural machinery and equipment design, Email: 1572423425@qq.com; **Shiyu Chen**, MS candidate, research interest: agricultural machinery and equipment design, Email: csy1997213@126.com; **Jianing Hu**, MS candidate, research interest: agricultural machinery and equipment design, Email:2531766957@qq.com; **Yong You**, PhD, Associate Professor, research interest: agricultural machinery and equipment design, Email: youyong@cau.edu.cn; **Decheng Wang**, PhD, Professor, research interest: agricultural machinery and equipment design, Email: wdc@cau.edu.cn.

***Corresponding author: Qing Zhang**, PhD, Associate Professor, research interest: intelligent agricultural equipment. College of Engineering, China Agricultural University, Beijing 100083, China. Tel: +86-15210513644, Email: zhangqingbit@cau.edu.cn.

established. In the end, the research indicated that the prototype model was suitable for optimizing the structure and the control strategy of the hydro-mechanical continuously variable transmission. Wang et al.[18,19] established the dynamics model of a two speed Automated Manual Transmission (AMT) of electric vehicle equipped with spring synchronizer in AMESim software. They also established a shift control model under the Matlab/Simulink environment. At last, simulation results based on dynamic model demonstrated that the spring synchronizer reduced the engagement time and vehicle impact. Mocera et al.[20] established the multibody model of tracked vehicle in ADAMS software to verify traction effects and optimize propulsion system controllers. Results indicated that the proposed model can be utilized for the optimal design of propulsion system controllers. Meng et al.[21] established a new AMT dynamic simulation model and evaluated its dynamic performance, which provided a model basis for improving the reliability of wheels in a harsh working environment. To conveniently analyze the dynamic performance of the tracked vehicles on soft pavement, Li et al.[22] established the tracked vehicle model. The results proved that the model presented in their study can be used to optimize the structural parameters of tracked vehicles. Bai et al.[23] conceived a multi-level adaptive lateral deformation crawler robot. The simulation verification of lateral force and traction force under different gripping teeth parameters was completed. Finally, the correctness of the theoretical model and the optimization of the grouser parameters was verified through prototype experiments. Qiao et al.[24,25] established a high-speed tracked vehicle action system model by using the simulation analysis method. Subsequently, the vibration response of the vehicle on uneven pavement was evaluated from four aspects: driver comfort, driver absorbed power, occupant handling efficiency, and suspension dynamic travel. It had reference significance for the prediction and evaluation of off-road maneuverability of high-speed tracked vehicles. The study demonstrated the value of using simulation analysis to improve the performance of such vehicles under different conditions. Ling et al.[26] established a parametric dynamic model of a tracked vehicle and proposed a parameter allocation objective function based on multi-index information fusion. Then, the virtual rolling processes of different insulation quilt lengths were analyzed under different thickness treatments. Lastly, the simulated results showed a satisfactory agreement with the experiment measurements, which suggested that the established model was an effective approach to evaluate and optimize the rolling machine.

However, there is little research on the dynamic model of the articulated steering half-track tractor, especially in the model verification of front wheel steering and articulated steering. In the study, an articulated steering half-track tractor was taken as the research object. The multi-body dynamics model of the whole tractor was established by RecurDyn. The validity and accuracy of the model was verified by combining theoretical analysis, model simulations and real vehicle tests.

2 Multi-body dynamics model construction and analysis

2.1 Topology analysis of the articulated steering half-track tractor

The main technical indexes of the tractor are as follows: The unloaded mass of the whole tractor is 1992.2 kg, the front body mass is 632.8 kg and the rear body mass is 1359.4 kg; The normal driving speed range is 3-6 km/h; The maximum climbing degree of tractor is 30°; The overall size of the tractor is 3100 mm× 1230 mm×1640 mm.

The whole tractor is mainly composed of frame, driving system, steering system, control system and power system. Among them, the driving system adopts the front axle wheel type and the rear axle track type arrangement. The track gauge of the rear crawler traveling system is 1140 mm and the track width is 300 mm, which mainly includes the driving wheels, guide tensioners, tensioners and rollers. The steering system consists of front wheel steering system and articulated steering system. The front wheel steering relies on hydraulic cylinders on the front axle to drive the steering mechanism. On the other hand, the articulated steering adopts universal transmission to transmit the power of the hydraulic system and the double oil cylinder is used to realize the steering movement.

According to the constraint relationship between the components, the topological structure of the articulated steering half-track tractor model can be seen in Figure 1, which also shows the connection relationship between the components of the articulated steering half-track tractor. It is clear that the interaction between components mainly includes revolute joint, contact force, driving torque, translate joint and spherical joint. J1, J2, J8, J16, and J17 are revolute joints between components. J3, J4, J6, J7, J10, J15, and J18 are contact forces. J5 is driving torque. J11 and J12 are spherical joints. J13 and J14 are translate joints.

The interaction between these components is listed in Table 1. The contact force J10 between the track and the ground is treated as contact-friction constraint. The driving torque J5 of the driving wheel is defined according to the specific working conditions. Other force constraints are treated as linear spring damping force.

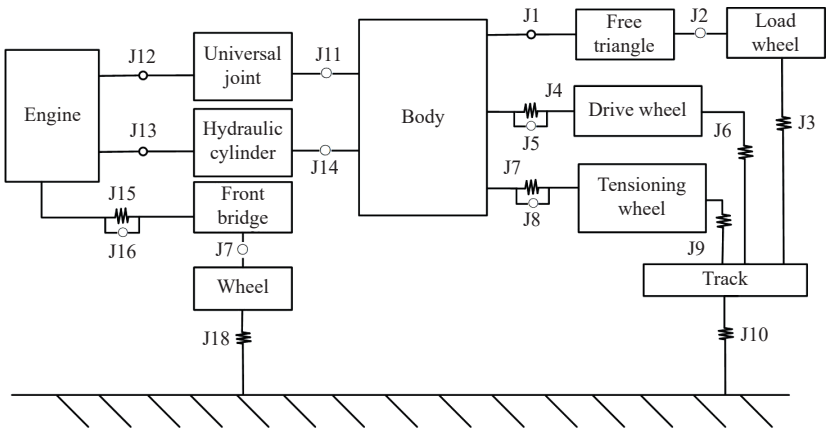

Figure 1 Topology diagram of the articulated steering half-track tractor

Table 1 Interactions between components

Number	Name	Quantity	Number	Name	Quantity
J1	Revolute joint	4	J10	Contact force	2
J2	Revolute joint	8	J11	Spherical joint	3
J3	Contact force	8	J12	Spherical joint	3
J4	Contact force	2	J13	Translate joint	2
J5	Driving torque	2	J14	Translate joint	2
J6	Contact force	2	J15	Contact force	1
J7	Contact force	2	J16	Revolute joint	1
J8	Revolute joint	2	J17	Revolute joint	2
J9	Contact force	2	J18	Contact force	2

2.2 Structural analysis of the steering system

In the study, the maximum articulated steering angle is 34°, and the maximum steering angle of the front axle inner wheel is 32°. Furthermore, the minimum turning radius of the front wheel steering is 4.0 m, and the minimum turning radius of the articulated steering is 2.2 m.

The structural diagram of the steering system is shown in Figure 2. Tractor steering system includes front wheel steering system and articulated steering system. There are two steering modes for the articulated steering half-track tractor: 1) When the tractor is operating in orchards with sufficient row spacing and row head space, the steering demand can be met by using only front wheel steering function; 2) When there are space constraints in the working environment and the steering demand cannot be met by using only front wheel steering, it is necessary to increase the use of articulated steering to meet the steering demand.

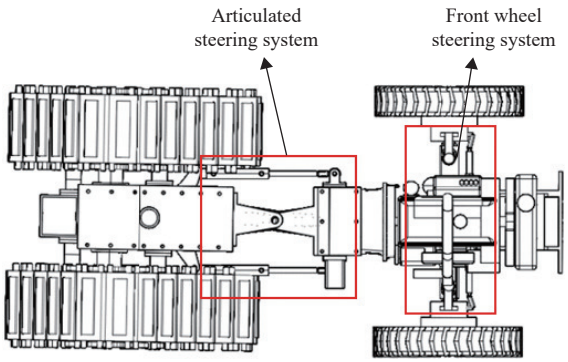

Figure 2 Structural diagram of the steering system

2.2.1 Front wheel steering system

The front wheel steering system is shown in Figure 3. The front wheel steering system consists of steering rocker arm, steering rocker arm, hydraulic rod, hydraulic cylinder and kingpin. Its steering principle is that during steering, the hydraulic cylinder supplies oil to push the hydraulic rod. The hydraulic rod drives the steering rocker arm and then drives the steering arm to make the wheel rotate around the kingpin.

2.2.2 Articulated steering system

The articulated steering system is shown in Figure 4. The articulated steering system consists of hydraulic rod, hydraulic cylinder and universal joint. The steering principle is that the articulated steering is completed through the synchronous expansion and contraction of two hydraulic cylinders. For example, during turning left, the hydraulic cylinder supplies oil to push the left hydraulic rod to shorten and the right hydraulic rod to elongate, so that the front and rear car bodies rotate around the universal joint and hinge joint.

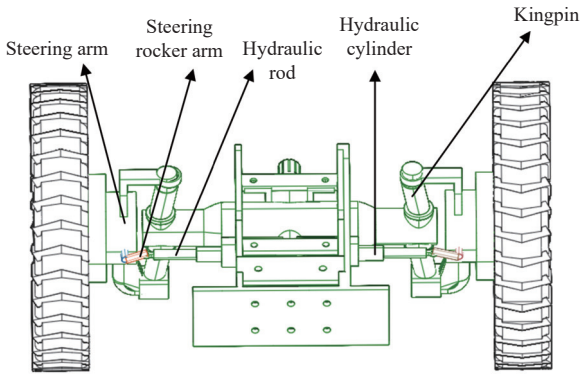

Figure 3 Front wheel steering system

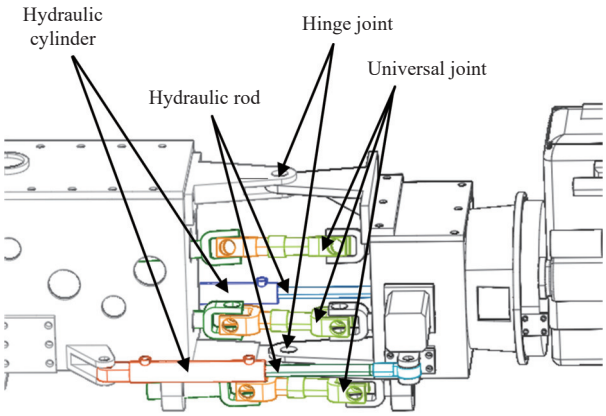

Figure 4 Articulated steering system

The relationship between hydraulic cylinder length and steering angle can be obtained through the conversion of geometric relationship. The construction of the geometric relationship diagram of the articulated steering is shown in Figure 5.

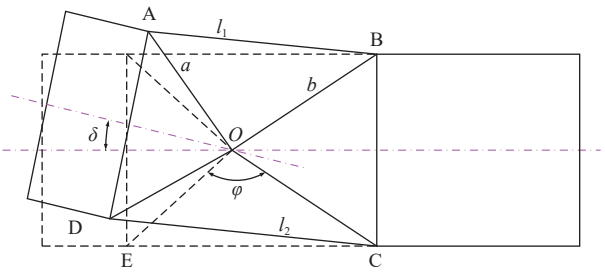

Figure 5 Geometric diagram of articulated steering

The front body rotates to the right around the hinge point O. According to the cosine theorem, the relationship between the length of the hydraulic cylinder and the bending steering angle can be obtained from Figure 5, as shown in Equation (1):

$$\begin{cases} l_1^2 = a^2 + b^2 - 2ab\cos(\varphi - \delta) \\ l_2^2 = a^2 + b^2 - 2ab\cos(\varphi + \delta) \end{cases} \quad (1)$$

where, δ is articulated steering angle, (°); a is length of OA (OE), m; b is length of OB(OC), m; φ is the angle between OA and OB, (°); l_1 is length of right cylinder AB, m; l_2 is length of left cylinder CD, m.

The length variation of the hydraulic cylinder is Δl. When the hydraulic cylinder is extended, Δl is positive, and Δl is negative when it is retracted. The relationship between the expansion amount of the cylinder at the extension end and the articulated steering angle is as shown in Equation (2). The relationship between the expansion amount of the cylinder at the contraction end and the

articulated steering angle is the same.

$$(L+\Delta l)^2 = a^2 + b^2 - 2ab\cos(\varphi+\delta) \tag{2}$$

The format of $\delta = f(\Delta l)$ as shown in Equation (3):

$$\delta = \arccos\left(\frac{a^2+b^2-(L+\Delta l)^2}{2ab}\right) - \varphi \tag{3}$$

2.2.3 Analysis of articulated steering process

The front wheels of the articulated steering half-track tractor first turn at the maximum angle. Then the body continues to rotate around the hinge joint for articulated steering, which further reduces the steering radius. The articulated steering process is shown in Figure 6.

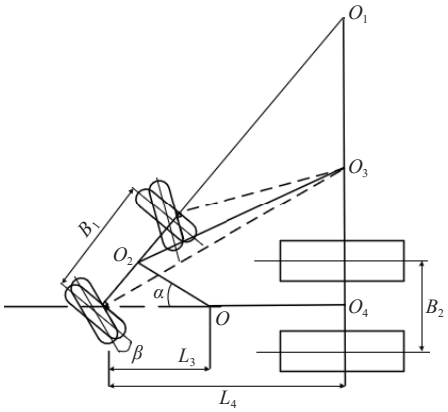

Note: O is the hinge point of the articulated steering, O_1 is the center of the steering radius under the maximum steering angle of the front wheel, O_2 is the symmetry center of the front axle, O_3 is the center of the minimum steering radius of the tractor, O_4 is the symmetry center of the rear half-track walking mechanism of the tractor, B_1 is the distance between the front wheels, B_2 is the distance between the rear track wheels.

Figure 6 Schematic diagram of articulated steering process

According to the geometric relationship in the Figure 6, Equations (4)-(7) can be obtained from the sine theorem:

$$\frac{O_1O_3}{\sin\beta} = \frac{O_1O_2}{\sin(180^\circ-\beta-\alpha)} \tag{4}$$

$$O_1O_2 = \frac{(L_4-L_3)+L_3\cos\alpha}{\sin\alpha} \tag{5}$$

$$O_1O_4 = \frac{(L_4-L_3)\cos\alpha+L_3}{\sin\alpha} \tag{6}$$

$$O_3O_4 = O_1O_4 - O_1O_3 \tag{7}$$

where, O_1O_2 is the distance from 1 to 2 m; O_1O_3 is distance from 1 to 3 m; O_1O_4 is distance from 1 to 4 m; O_3O_4 *is* distance from 3 to 4 m; L_3 is the distance from the hinge point to the front wheel center, m; L_4 is the vehicle wheelbase, m; α is the maximum angle of articulated steering, (°); β is the maximum steering angle of the front wheel, (°).

According to the geometric analysis of the articulated steering process, the symmetrically arranged articulated steering cylinders should be arranged with the hinge point as the midpoint of the cylinder as far as possible, so that the extension and retraction of each cylinder are as same as possible when the tractor turns This is also conducive to the reliable use of the articulated steering mechanism. According to the steering mechanics analysis, the steering torque of this arrangement scheme is the minimum.

2.3 Kinematics analysis of articulated steering

In the process of articulated steering, first turn the front wheels to the maximum angle and then articulated steering. In order to obtain the kinematic equations of the articulated steering tractor, the following assumptions are made[27,28]. The articulated steering angle φ remains constant under small displacement. The track length does not change during driving. There is no slip between the track and the track wheel. The dynamic effect caused by low speed is ignored. According to the structure of the articulated steering tractor, the kinematics relationship of the articulated steering process is constructed as shown in Figure 7.

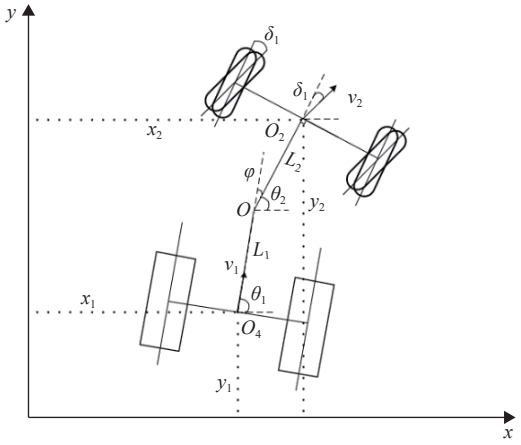

Figure 7 Articulated steering kinematic relationship of the articulated steering tractor

where, L_1 is the distance from the hinge point to the rear axle, m; L_2 is the distance from the hinge point to the front axle, m; δ_1 is the maximum value of the front wheel turning angle, (°); φ is the articulated steering angle, (°); θ_1 is the azimuth angle of the rear body, (°); θ_2 is the azimuth angle of the front body (°); v_1 is the center speed of the rear axle (m/s); v_2 is the center speed of the front axle (m/s).

The kinematic constraints of the articulated steering tractor can be expressed as Equation (8).

$$\begin{cases} \dot{x}_1\sin\theta_1 - \dot{y}_1\cos\theta_1 = 0 \\ \dot{x}_2\sin\theta_2 - \dot{y}_2\cos\theta_2 = 0 \end{cases} \tag{8}$$

where, $\dot{x}_1$ is the component of v_1 in the *X*-axis direction, m/s; $\dot{y}_1$ is the component of v_1 in the *Y*-axis direction, m/s; $\dot{x}_2$ is the component of v_2 in the *X*-axis direction, m/s; $\dot{y}_2$ is the component of v_2 in the *Y*-axis direction, m/s.

The relationship between the change rate of articulated steering angle and the change rate of front and rear body azimuth angle is shown in Equation (9).

$$\dot{\varphi} = \dot{\theta}_1 - \dot{\theta}_2 \tag{9}$$

where, $\dot{\varphi}$ is rate of change of bending steering angle, rad/s; $\dot{\theta}_1$ is rate of change of the rear body azimuth, rad/s; $\dot{\theta}_2$ is rate of change of the front body azimuth, rad/s,

The relative velocity equations of the front and rear bodies are shown in Equation (10).

$$\begin{cases} v_1\cos\varphi = v_2\cos\delta_1 + \dot{\theta}_1L_1\sin\varphi \\ v_1\sin\varphi = \dot{\theta}_2L_2 + \dot{\theta}_1L_1\cos\varphi + v_2\sin\delta_1 \end{cases} \tag{10}$$

The rate of change of the rear body azimuth is shown in Equation (11).

$$\dot{\theta}_1 = \frac{(\sin\varphi - \tan\delta_1\cos\varphi)v_1 + \dot{\varphi}L_2}{L_1(\cos\varphi + \tan\delta_1\sin\varphi) + L_2} \tag{11}$$

In the proposed method, the variable is the rate of change of the articulated angle, denoted by ω. The articulated steering kinematic model can be expressed as Equation (12).

$$\begin{bmatrix} \dot{x}_1 \\ \dot{y}_1 \\ \dot{\theta}_1 \\ \dot{\varphi} \end{bmatrix} = \begin{bmatrix} \cos\theta_1 & 0 \\ \sin\theta_1 & 0 \\ \dfrac{(\sin\varphi - \tan\delta_1\cos\varphi)}{L_1(\cos\varphi + \tan\delta_1\sin\varphi) + L_2} & \dfrac{L_2}{L_1(\cos\varphi + \tan\delta_1\sin\varphi) + L_2} \\ 0 & 1 \end{bmatrix} \begin{bmatrix} v_1 \\ \omega \end{bmatrix} \tag{12}$$

This matrix can be used to calculate the minimum turning radius, as well as the required front wheel and bending angle for subsequent steering simulation.

2.4 Dynamic analysis of articulated steering

In the section, the steering dynamics analysis is carried out based on the front wheel steering angle of the articulated steering half-track tractor reaches the maximum steering angle and the front wheel steering mechanism is locked. The key to vehicle steering process is steering thrust, which is affected by the steering resistance moment of the vehicle. The maximum value of the vehicle steering resistance moment occurs in the static in-situ steering condition, so this section analyzes the in-situ steering dynamics. Because the rear axle is crawler arrangement which has a great impact on steering, this study analyzes the effect of rear axle crawler on the steering dynamics.

Due to the symmetrical arrangement of the rear half of the travel mechanism, it is assumed that the weight of the rear half of the tractor body is equally distributed to both sides. The grounding pressure on the tracked micro elements is calculated according to Equation (13).

$$p_i = \frac{G_i}{\mathrm{d}x\mathrm{d}y} = \frac{m_2 g}{2\mathrm{d}x\mathrm{d}y} \tag{13}$$

where, p_i is the grounding pressure on the tracked micro elements, N/m^2; G_i is the weight of each half-track walking mechanism, N; i is L or R represents left and right, respectively; g is acceleration of gravity, N/kg; m_2 is the mass of the rear half car body, kg; dx is the micro element in the length direction of the part of the track contacting the ground, m; dy is the micro element in the width direction of the part of the track contacting the ground, m.

The friction resistance of the part of the track contacting the ground in the length direction and width direction are shown in Equations (14) and (15), respectively.

$$F_{ix} = \iint \mathrm{d}F_{ix}\mathrm{d}x\mathrm{d}y = \int_{A_i-\frac{1}{2}b}^{A_i+\frac{1}{2}b} \mathrm{d}y \int_{-\left(\frac{1}{2}a-B_i\right)}^{\frac{1}{2}a+B_i} \frac{1}{2}\mu m_2 g \frac{y}{\sqrt{x^2+y^2}}\mathrm{d}x \tag{14}$$

$$F_{iy} = \iint \mathrm{d}F_{iy}\mathrm{d}x\mathrm{d}y = \int_{A_i-\frac{1}{2}b}^{A_i+\frac{1}{2}b} \mathrm{d}y \int_{-\left(\frac{1}{2}a-B_i\right)}^{\frac{1}{2}a+B_i} \frac{1}{2}\mu m_2 g \frac{x}{\sqrt{x^2+y^2}}\mathrm{d}x \tag{15}$$

where, F_{ix} is the friction resistance in the length direction, N; F_{iy} is the friction resistance in the width direction, N; a is the length of the track contacting the ground, m; b is the width of the track contacting the ground, m; μ is the coefficient of friction of the ground; A_i is the longitudinal offset of the instantaneous center of track speed, m; B_i is the lateral offset of the instantaneous center of track speed, m.

In the steering process, the tracked chassis rotates around the geometric center of the ground contacting part of the track. The frictional resistance between the ground and the tractor's tracked travel mechanism generates a friction resistance moment with the ground contacting part of the track as the geometric center, as shown in Equation (16).

$$M_i = \iint \left(|y - A_i|\mathrm{d}F_{ix} + |x - B_i|\mathrm{d}F_{iy}\right)\mathrm{d}x\mathrm{d}y = \int_{A_i-\frac{1}{2}b}^{A_i+\frac{1}{2}b} \mathrm{d}y \int_{-\left(\frac{1}{2}a-B_i\right)}^{\frac{1}{2}a+B_i} T\mathrm{d}x \tag{16}$$

where, M_i is the friction resistance moment, N·m; $T = \frac{1}{2}\mu m_2 g \cdot \frac{y|y-A_i| + x|x-B_i|}{\sqrt{x^2+y^2}}$.

This steering resistance moment equation provides the required steering driving moment for the subsequent steering simulation and affects the setting of road characteristic parameters.

2.5 Construction of the multi-body dynamics model

Combined with the topological structure of the articulated steering half-track tractor, a multi-body dynamic model is built for its track system, front wheel steering system and the articulated steering system, as shown in Figure 8.

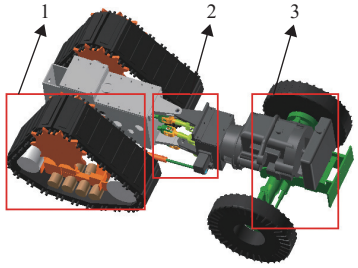

1.Track system 2. Articulated steering system 3. Front wheel steering system

Figure 8 Articulated steering half-track tractor multi-body dynamics model

3 Construction of hard pavement and farmland soft pavements

3.1 Construction of the pavement spectrum model

Road roughness plays an significant role in vehicle road system simulation. The statistical characteristics of road roughness are mainly expressed using the road power spectral density. According to the GB/T 7031-2005 "Mechanical vibration road pavement spectrum measurement data report"[29], the fitting expression for pavement power spectral density is shown in Equation (17).

$$G_q(n) = G_q(n_0)\left(\frac{n}{n_0}\right)^{-W} \tag{17}$$

where, n is the spatial frequency, m^{-1}; n_0 is the reference spatial frequency, n_0=0.1 m^{-1}; $G_q(n)$ is the power spectral density corresponding to the spatial frequency n of road roughness, m^3; $G_q(n_0)$ is the standard power spectral density corresponding to the reference spatial frequency n_0 of road roughness, m^3; W is the frequency index, W=2.

In this study, the harmonic superposition method is used to simulate this random process. The main principle is that when the road roughness coefficient is given, the road roughness can be composed of the superposition of multiple sine and cosine functions. The unevenness curve of the road surface spectrum is taken into consideration, along with the actual speed factor. According to the actual speed v, the spatial frequency spectral density $G_q(n)$ is converted to the time power spectrum function $G_q(f)$, as shown in Equation (18).

$$G_q(f) = \frac{1}{v} G_q(n) \tag{18}$$

where, f is the time frequency, $f = vn$ (Hz); v is the vehicle speed, m/s.

According to the power spectral density expansion property of stationary random process, the variance of road roughness can be expressed as shown in Equation (19).

$$\sigma_x^2 = \int_{f1}^{f2} G_q(f)\,\mathrm{d}f \tag{19}$$

where, f_1 to f_2 are divided into multiple cells m, and the spectral density value $G_q(f)$ on each cell is replaced by the spectral density value $G_q(f_{\mathrm{mid}\_n})$ of frequency f_{mid_n} at the center of the interval. Equation (19) can be written as Equation (20).

$$\sigma_x^2 = \sum_{n=1}^{m} G_{\mathrm{q}}\left(f_{\mathrm{mid}\_n}\right)\Delta f_n \tag{20}$$

where, Δf_n is frequency value of the nth segment, Hz.

For each frequency f_{mid_n}, the standard deviation is shown in Equation (21).

$$\sigma_{\mathrm{f_{mid}}\_n} = \sqrt{G_{\mathrm{q}}\left(f_{\mathrm{mid}\_n}\right)\Delta f_n} \tag{21}$$

There are sine wave functions as shown in Equation (22).

$$f(t) = \sigma_{f_{\mathrm{mid}\_n}} \sin\left(2\pi f_{\mathrm{mid}\_n} t + \varepsilon_n\right) \tag{22}$$

where, Δf_n is frequency value of the n^{th} segment, Hz; ε_n is a random number uniformly distributed on [0, 2π]; t is time, s; x is vehicle longitudinal displacement, m.

The sine wave functions corresponding to each cell are superimposed to obtain the random road irregularity input in the time domain as shown in Equation (23).

$$q(x) = \sum_{k=1}^{m} \sqrt{2}\sigma_{f_{\mathrm{mid}\_n}} \sin\left(2\pi f_{\mathrm{mid}\_n} t + \varepsilon_n\right) \tag{23}$$

According to GB/T 7031-2005 “Mechanical vibration road surface spectrum Measurement data Report” standard, cement hard pavement belongs to grade B and farmland soft pavement belongs to grade E. The B and E random pavements are simulated in Matlab, and the constructed pavement model along with their power spectra are illustrated in Figures 9 and 10.

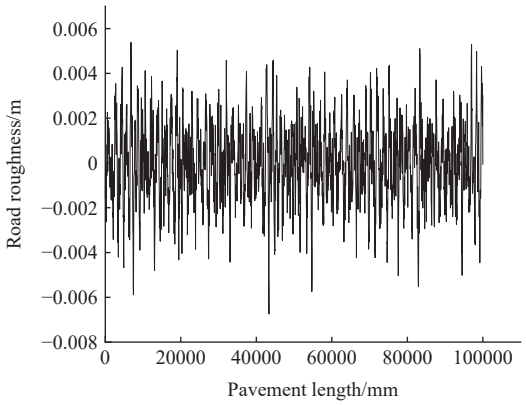

a. Roughness of hard pavement (Grade B pavement)

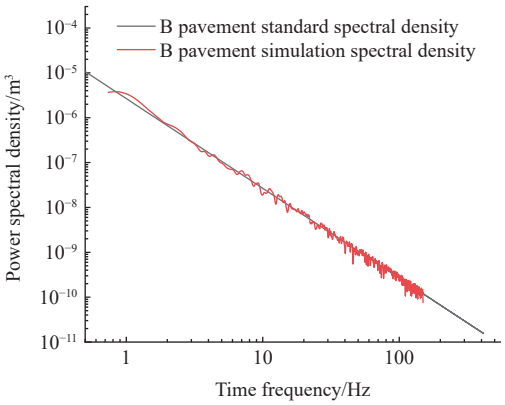

b. Power spectrum of hard pavement (Grade B pavement)

Figure 9 Pavement model

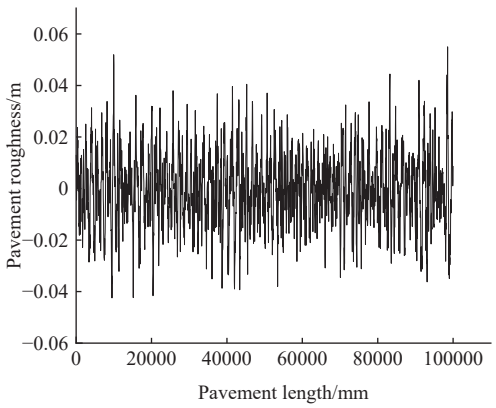

a. Roughness of soft pavement (Grade E pavement)

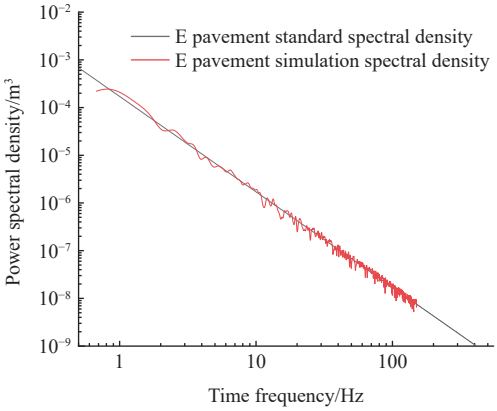

b. Power spectrum of soft pavement (Grade E pavement)

Figure 10 Pavement model

According to the power spectrum of B and E pavement, it can be concluded that the error between B pavement and standard B pavement constructed by Matlab simulation is 6.4%, while the error between E pavement and standard E pavement is 7.1%. The fitting degree is excellent, indicating that the constructed pavement model possesses high accuracy and reliability, which makes it suitable for subsequent simulation experiments.

3.2 Setting of pavement parameters

Combined with the real vehicle test environment, the cement hard pavement and farmland soft pavement models were constructed in the dynamic software. The characteristic parameters were set as listed in Table 2. In the software, it is assumed that the hard pavement will not be deformed by the rolling of the tracks. Baker’s pressure-settlement model was used to simulate the

farmland soft pavement in a sandy loam environment.

4 Results and discussion

Based on the constructed simulation model, the simulations were carried out in the dynamic software while the road parameters were set according to Table 2. In order to obtain real-time tractor speed and position, a real tractor test was conducted on an articulated steering half-track tractor with a navigation mobile station installed on the roof.

Table 2 Characteristic parameters of hard and farmland soft simulated pavement

Pavement type	Parameter	Value
Hard pavement	Ground stiffness/(N·m^{-1})	10 000
	Damping coefficient/(N·m^{-1}·s^{-1})	10.0
	Maximum friction factor	0.7
	Pavement deformation index	2
Soft pavement	Pavement deformation index	0.7
	Cohesive deformation modulus/(kN·m^{-n-1})	4.18
	Friction deformation modulus/(kN·m^{-n-2})	1.20
	Soil cohesion/kPa	1.72
	Internal friction angle of soil/(°)	29
	Soil shear modulus/cm	0.25

4.1 Straight line speed verification

The straight-line speed simulation and test of the articulated steering tractor were carried out on hard pavement and farmland soft pavement, respectively. The test environment was shown in Figure 11. Both simulation and test speed were 1.5 m/s.

a. Hard pavement test environment

b. Farmland soft pavement test environment

Figure 11 Test environment

Data were acquired after simulation and test, and created speed comparison plots, as shown in Figures 12 and 13:

After analyzing the data, the speed error was obtained as listed in Table 3.

It can be seen from the Table 3 that the average speed of the test is slightly higher than the average speed of the simulation. The average speed error of both is less than 3%. It can be seen from Figure 12 that although the speed fluctuation in the test is greater than in the simulation, the overall speed fluctuation of both tests remained relatively consistent.

The speed errors in Table 4 were obtained by analyzing the data in Figure 13.

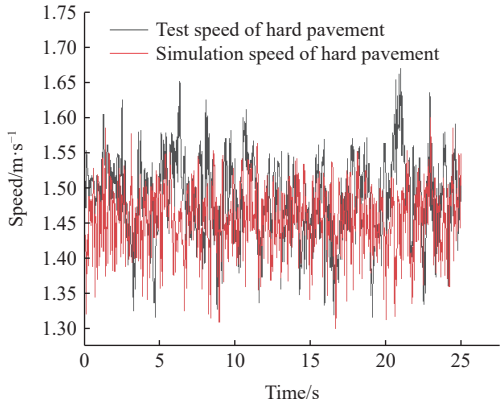

Figure 12 Speed comparison of hard pavement

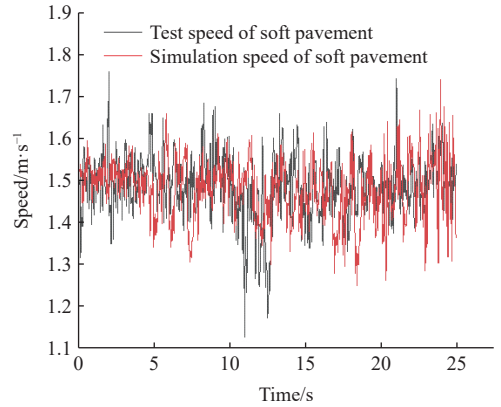

Figure 13 Speed comparison of farmland soft pavement

Table 3 Hard pavement speed error analysis (m/s)

Group	Simulation	Test
Maximum speed	1.59	1.66
Minimum speed	1.30	1.31
Average velocity	1.46	1.48
Standard deviation	0.048	0.059
Error	2.7%	1.4%

Table 4 Farmland soft pavement speed error analysis (m/s)

Group	Simulation	Test
Maximum speed	1.74	1.76
Minimum speed	1.24	1.13
Average velocity	1.47	1.48
Standard deviation	0.073	0.076
Error	2.1%	1.4%

Table 4 reveals that the average speed of the test is slightly higher than the average speed of the simulation, the average speed error is less than 3%. It can be further deduced from the standard deviation that the overall speed fluctuation of the two tests is small, but there are large fluctuations in the speed of individual points in the simulation and test, which means that the pavement has large fluctuations at these points and thus causes speed fluctuations. However, these fluctuations have relatively little impact on the overall test.

4.2 Straight-line driving offset verification

Simulation and experimental tests of the straight-line driving offset were performed on both hard pavement and farmland soft

pavement to verify the straight-line driving stability of the articulated steering half-track tractor and provide a basis for subsequent unmanned driving. The test settings are as follows: Using the marker line to take the left front of the track as the starting point, marking 20 m forward along the track direction as the end point. The hard pavement test is shown in Figure 11a, the white line is the marking line. The farmland pavement test is shown in Figure 11b, the marker line is the center line between the ground; The crawler chassis advances at a speed of 1.5 m/s; Three tests for each pavement; The driver will adjust the direction at the initial moment and will not operate the steering wheel during driving. The comparison data of simulation and test are listed in Table 5.

Table 5 Comparison of driving offset between hard and farmland soft pavement (mm)

Group	Hard pavement offset		Soft pavement offset	
	Front wheel	Rear wheel	Front wheel	Rear wheel
Simulation1	404.5	312.4	600.4	550.1
Simulation2	423.6	323.2	584.5	527.4
Simulation3	384.5	301.5	612.3	551.6
Average value	404.2	312.4	599.1	543.0
Test1	431.2	314.5	604.8	540.1
Test2	414.5	302.1	556.4	514.5
Test3	386.4	283.6	584.5	526.3
Test	410.7	300.1	581.9	527.0
Error	1.6%	3.9%	3.8%	2.4%

It can be seen from Table 5 that on hard pavement, the front wheel travel offset of simulation and test is 404.2 mm and 410.7 mm, with an error of 1.6%, the rear wheel travel offset is 312.4 mm and 300.1 mm, with an error of 3.9%; On the farmland soft pavement, the simulated and test of front wheel travel offset is 599.1 mm and 581.9 mm, with an error of 3.8%, the rear wheel travel offset is 543.0 mm and 527.0 mm, with an error of 2.4%.

GB/T 15370.4 “General technical conditions of agricultural tractors Part 4: Crawler tractors”[30] stipulates that the deviation of crawler tractors on a dry, hard and flat pavement with a longitudinal and transverse slope not more than 1% should not be more than 6%. The simulation and test results in this study meet this requirement.

4.3 Steering performance verification

The steering simulation and test were carried out for the articulated steering tractor. The test settings were as follows: The tractor turned continuously for 2 turns in the simulation environment and test environment, the position data was recorded through the navigation mobile station.

4.3.1 Performance verification of front wheel steering

When performing front wheel steering, the front wheels were turned to maximum angle without articulated steering. During the steering simulation, the steering path diagram was drawn based on the walking track of the track centers on both sides, as shown in Figure 14. During the steering test, draw the steering path diagram with the indentation center of the tracks on both sides, as shown in Figure 15.

Tractor position information was extracted after the simulation and test. Taking the starting point of the vehicle as the 0 position point, and a relative position comparison diagram was built as shown in Figure 16.

As shown in Figure 16, each wave peak to wave trough constitutes half a turn of the vehicle which can get a turning radius. Both simulation and test can get 4 turning radius. The comparison of front wheel turning radius is listed in Table 6.

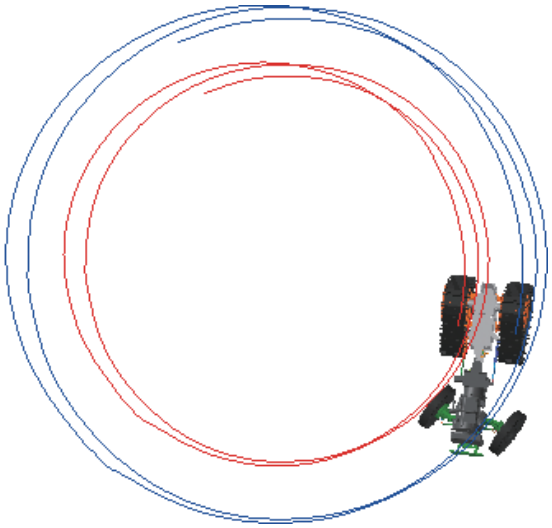

Figure 14 Front wheel steering simulation track

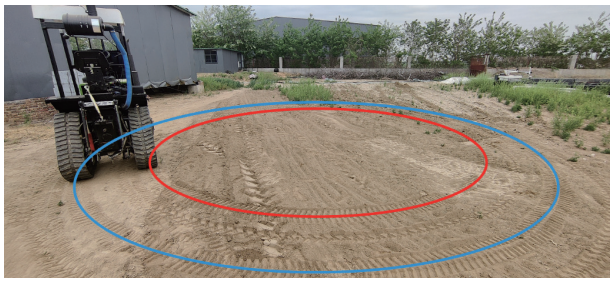

Figure 15 Front wheel steering test track

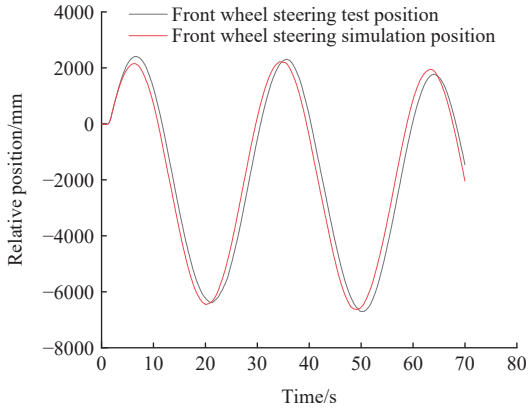

Figure 16 Relative position of front wheel steering vehicle

Table 6 Comparison table of turning radius of front wheel steering

Group	Simulation/mm	Test/mm
1	4291.5	4373.0
2	4323.2	4321.3
3	4420.0	4493.5
4	4283.4	4219.5
Average value	4329.5	4351.8
Error range	7.1%-10.5%	5.5%-12.3%

It can be seen from Table 6 that the average value of the simulation turning radius of the front wheel steering is 4329.5 mm and the average value of the test turning radius is 4351.8 mm. The theoretical front wheel steering radius of articulated steering half-track tractor is 4 m. The simulation turning radius error is 8.2% and the test turning radius error is 8.7%, both of which are less than 10%. Therefore, the established model is highly accurate and reliable.

It can be seen from Figure 16 the lateral sliding of the tractor occurred in the lateral position during the steering process. The sliding width can be obtained by analyzing the position changes of three peaks and two troughs as listed in Table 7.

Table 7 Front wheel steering lateral deviation (mm)

Group	Simulation	Test
Peak 1-2	64.0	103.5
Peak 2-3	272.0	330.2
Trough 1-2	192.9	344.5
Average value	176.3	259.4
Error	4.1%	6.0%

The average lateral deviation between the end point and the starting point after one revolution of the front wheel steering simulation is 176.3 mm, and the average lateral deviation of the test is 259.5 mm. The error of the simulation and the test are 4.1% and 6.0%. It can be seen from the Table 7 that some positions exhibit significant sliding during the simulation and test, which means that the road conditions fluctuate greatly within a certain range.

4.3.2 Performance verification of articulated steering

The front wheel turned to the maximum angle during the articulated steering, while the articulated mechanism also turned to the maximum angle. During the steering simulation, the steering path diagram was drawn based on the walking track of the track centers on both sides, as shown in Figure 17. During the steering test, draw the steering path diagram with the indentation center of the tracks on both sides, as shown in Figure 18.

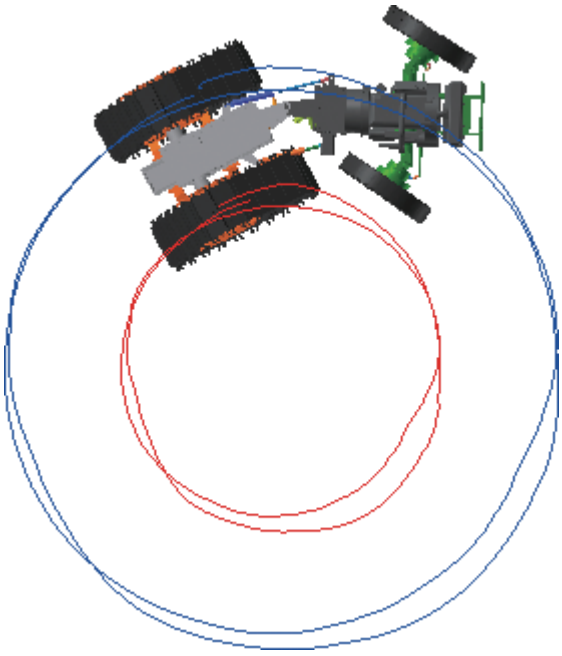

Figure 17 Articulated steering simulation track

Figure 18 Articulated steering test track

Tractor position information was extracted after the simulation and test. Taking the starting point of the vehicle as the 0 position point, and a relative position comparison diagram was built as shown in Figure 19. The comparison of articulated steering radius is listed in Table 8.

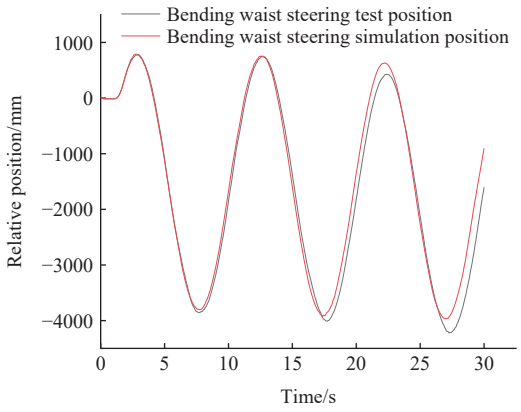

Figure 19 Relative position of articulated steering vehicle

Table 8 Comparison table of turning radius of articulated steering (mm)

Group	Simulation	Test
1	2294.5	2311.6
2	2277.5	2297.6
3	2378.3	2323.5
4	2312.9	2164.0
Average value	2315.8	2274.2
Error range	3.5%-8.1%	1.6%-5.6%

It can be seen from Table 8 that the average value of the simulation turning radius of the front wheel steering 2315.8 mm and the average value of the test turning radius is 2274.2 mm. The theoretical steering radius of the articulated steering of articulated steering half-track tractor is 2.2 m. The error of the simulated turning radius is 5.3% and the error of the test turning radius is 3.4%, both of which are less than 5%. Therefore, the established model is more accurate and credible than the front wheel steering when articulated steering.

Similarly, lateral sliding occurred in the lateral position of the tractor during the articulated steering process. The sliding width can be obtained by analyzing the changes in the positions of the three peaks and two troughs, as listed in Table 9.

Table 9 Lateral deviation of articulated steering (mm)

Group	Simulation	Test
Peak 1-2	34.3	28.5
Peak 2-3	130.2	351.0
Trough 1-2	201.8	54.0
Average value	122.1	144.5
Error	5.2%	6.4%

The average lateral deviation between the end point and the starting point after one revolution of the articulated steering simulation is 122.1 mm, and the average lateral deviation of the test is 144.5 mm. The larger lateral deviation of peak 2-3 in the test verification is due to the large angle of the articulated steering and the less flat road surface. The error of simulation and test are 5.2% and 6.4%, respectively. The error is small, which indicates that established model has high accuracy and reliability.

5 Conclusions

In the study, in order to research the kinematics and dynamics characteristics of the articulated steering half-track tractor, the multi-body dynamics model of the tractor was constructed and verified by the combination of theoretical analysis and experimental data. The specific conclusions can be drawn as follows:

1) On both hard and soft farmland pavements, the average speed errors of the dynamic model were found to be 2.7% and 2.1%, respectively. At the same time, the straight-line driving offset errors of the front wheel were 1.6% and 3.8%, and the rear wheel were 3.9% and 2.4%. It indicated that the multi-body dynamics model of the articulated steering half-track tractor has high accuracy in straight travel.

2) Compared with the test data, the turning radius error of the constructed multibody dynamic model in front wheel steering process was 8.2%. On the other hand, the turning radius error in the articulated steering process was 5.3%. It showed that the constructed multi-body dynamics model of the articulated steering tractor has high accuracy.

3) The comparison of simulation and test data under multiple working conditions indicated that the constructed multi-body dynamics simulation model of the articulated steering tractor had high accuracy in simulating the straight and turning processes which can provide a reference model for subsequent path tracking research.

Acknowledgements

This work was financially supported by the National Key R&D Program of China (Grant No. 2022YFD2202102).

[References]

[1] Han H W, Han J S, Chung W J, Kim J T, Park Y J. Prediction of synchronization time for tractor power-shift transmission using multi-body dynamic simulation. Transactions of the ASABE, 2021; 64(5): 1483–1498.

[2] Gao Y, Cao D P, Shen Y H. Path-following control by dynamic virtual terrain field for articulated steer vehicles. Vehicle System Dynamics, 2020; 58(10): 1528–1552.

[3] Jin Y H, Yuan Y W, Zhu L C, Wang D C, Zhao B, Fang X F. Design and optimization of an automatic hydraulic steer-by-wire system for an agricultural chassis. Int J Agric & Biol Eng, 2022; 15(1): 132–138.

[4] Ahn D V, Shin I K, Oh J, Chung W J, Han H W, Kim J T, et al. Reduction of torsional vibration in resonance phenomena for tractor power take-off drivelines using torsional damper. Transactions of the ASABE, 2021; 64(2): 365–376.

[5] Li H, Zhao Y Q, Qin C B, Ding L, Cheng S S, Zhang K F. Design and test of the control system of the folding steering unmanned plant protection vehicle. Journal of Agricultural Machinery, 2020; 51(S2): 544–553. (in Chinese)

[6] Kim W S, Kim Y S, Kim Y J. Development of prediction model for axle torque of agricultural tractors. Transactions of the ASABE, 2020; 63(6): 1773–1786.

[7] Cui L F, Mao H P, Xue X Y, Ding S M, Qiao B Y. Optimized design and test for a pendulum suspension of the crop spray boom in dynamic conditions based on a six DOF motion simulator. Int J Agric & Biol Eng, 2018; 11(3): 76–85.

[8] Bruno F, Valda R, Enrico C. Lateral stability performance of articulated narrow-track tractors. Agronomy, 2021; 11(12): 2512–2512.

[9] Oh J, Chung W J, Han H W, Kim J T, Son G, Park Y J. Evaluation of tractor ride vibrations by cab suspension system. Transactions of the ASABE, 2020; 63(5): 1465–1476.

[10] Zhao C H, Yang Z Y, Cheng X R, Hu J W, Hou X L. SINS/GNSS integrated navigation system based on maximum versoria filter. Chinese Journal of Aeronautics, 2022; 35(8): 168–178.

[11] Hu K, Zhang W Y, Kun L. Multi-body dynamics modeling and test of triangular crawler chassis with high clearance. Transactions of the CSAM, 2021; 52(7): 386–394. (in Chinese)

[12] Liu L, Zhang T, Xie N. Multi-body dynamics modeling and verification of small agricultural crawler chassis. Transactions of the CSAE, 2019; 35(7): 39–46. (in Chinese)

[13] Liu L, Xie N, Zhang T. Mechanical modeling and driving performance analysis of tracked vehicle on farmland soft slope. Mechanical Design, 2021; 38(3): 110–118. (in Chinese)

[14] Ma X G, Pan S W, You X M. Mathematical model of crawler driving system and tension calculation. Vibration and Impact, 2014; 33(3): 186–190. (in Chinese)

[15] Hao B F, Wang H Y, Rui Q. Dynamic modeling and model test verification of tank multibody system. China Mechanical Engineering, 2018; 29(4): 429–433, 440. (in Chinese)

[16] Xie H, Wang H Y, Hao B F. Dynamic modeling and model test verification of tracked vehicles. Agricultural Equipment and Vehicle Engineering, 2018; 56(6): 44–48. (in Chinese)

[17] Wu W, Luo J L, Wei C H, Yuan S H. Design and control of a hydro-mechanical transmission for all-terrain vehicle. Mechanism and Machine Theory, 2020; 154: 104052.

[18] Wang Y W, Wu J L, Zhang N, Mo W W. Dynamics modeling and shift control of a novel spring-based synchronizer for electric vehicles. Mechanism and Machine Theory, 2022; 168: 104586.

[19] Rakun J, Pantano M, Lepej P, Lakota M. Sensor fusion-based approach for the field robot localization on Rovitis 4.0 vineyard robot. Int J Agric & Biol Eng, 2022; 15(6): 91–95.

[20] Francesco M, Aurelio S, Andrea N. Grousers effect in tracked vehicle multibody dynamics with deformable terrain contact model. Applied Science-Basic, 2020; 10(18): 6581.

[21] Meng D L, Tian M J, Miao L Y, Wang Y H, Hu J L, Gao B Z. Design and modeling of an in-wheel two-speed AMT for electric vehicles. Mechanism and Machine Theory, 2021; 163: 104383.

[22] Li Y L, Tang C. Research on coupled dynamic model of tracked vehicles and its solving method. Mathematical Problems in Engineering, 2015; 2015(Pt.4): 293125.1–293125.10.

[23] Bai Y D, Sun L Y, Zhang M L. Terramechanics modeling and grouser optimization for multistage adaptive lateral deformation tracked robot. IEEE Access, 2020; 8: 171387–171396.

[24] Qiao X Y, Jin Y, Gu C. Vibration response and evaluation method of high-speed tracked vehicles driving off-road. Shock and Vibration, 2022; 2022: 2866236.

[25] Li Y M, Liu Y, Yue X, Li Z Q, Liu X A, Li T L. Mechanical model for double side self-propelled rolling machine based on rigid and flexible contact dynamics. Int J Agric & Biol Eng, 2022; 15(6): 38–43.

[26] Ling Q H, Dai J C, He X Y, Chen S Z, Chen Z W. Allocation optimization of multi-axis suspension dynamic parameter for tracked vehicle. Complexity, 2021; 2021: 8961020.

[27] Liu J Z, Li P P, Mao H P. Mechanical and kinematic modeling of assistant vacuum sucking and pulling operation of tomato fruits in robotic harvesting. Transactions of the ASABE, 2015; 58(3): 539–550.

[28] Lee D H, Choi C H, Chung S O, Kim Y J, Lee K H, Shin B S. Development of a plow tillage cycle for an agricultural tractor. Transactions of the ASABE, 2016; 59(2): 445–454.

[29] China standard. GB/T 7031-2005: Machinery Industry Federation. Measurement data report of mechanical vibration road pavement spectrum. Beijing, China: Standards Publishing House, 2005. (in Chinese)

[30] China standard. GB/T 15370.4-2012: Machinery Industry Federation. General technical conditions for agricultural tractors. Beijing, China: Standards Publishing House, 2012. (in Chinese)